Trans. JSASS Aerospace Tech. Japan
Vol. 9, pp.1-8, 2011

Effect of Atomic Oxygen Exposure on Surface Resistivity Change of Spacecraft Insulator Material

By Noor Danish Ahrar MUNDARI, Arifur Rahman KHAN, Masaru CHIGA, Teppei OKUMURA*, Hirokazu MASUI, Minoru IWATA, Kazuhiro TOYODA and Mengu CHO

Kyushu Institute of Technology, Kitakyushu, Japan

(Received July 6th, 2010)

Spacecraft surface charging can lead to arcing and a loss of electricity generation capability in solar panels or even loss of a satellite. The charging problem may be further aggravated by atomic oxygen (AO) exposure in Low Earth orbits, which modifies the surface of materials like polyimide, Teflon, anti-reflective coatings, cover glass etc, used on satellite surfaces, affecting materials properties, such as resistivity, secondary electron emissivity and photo emission, which govern the charging behavior. These properties are crucial input parameters for spacecraft charging analysis. To study the AO exposure effect on charging governing properties, an atomic oxygen exposure facility based on laser detonation of oxygen was built. The facility produces AO with a peak velocity value around 10-12km/s and a higher flux than that existing in orbit. After exposing the polyimide test material to the equivalent of 10years of AO fluence at an altitude of 700-800km, surface charging properties like surface resistivity and volume resistivity were measured. The measurement was performed in a vacuum using the charge storage decay method at room temperature, which is considered the most appropriate for measuring resistivity for space applications. The results show that the surface resistivity increases and the volume resistivity remains almost the same for the AO exposure fluence of 5.4×10^{18} atoms cm^{-2}.

Key Words: Spacecraft Charging, Surface Resistivity, Volume Resistivity, Surface Charge Decay Method, Polyimide

1. Introduction

Since the late 1990s, the size of telecommunication satellites has increased drastically in line with the demand for more communication capacitance and an increasing number of satellite TV channels. To save the launch costs by keeping the number of launches low, the number of transponders per satellite has increased. Satellite power level has also been increased. Today's major commercial telecommunication satellites consume more than 10kW. In order to mange increasing power needs more efficiently, photovoltaic generation and transmission voltage are being increased as well. Satellite bus voltage has been increased from 50V, used commonly by previous satellites, to 100V.

As the satellite voltage increased, accidents related to solar arrays began to occur very frequently. The accidents were mostly due to arcing and subsequent short-circuiting of array circuits, causing in the worst case, total loss of satellite functions. These accidents were not limited to geosynchronous Earth orbit (GEO) satellite, as polar Earth orbit (PEO) satellite has also been affected. One example was the total loss of ADEOS- 2 in 2003.[1)]

The central theme of spacecraft charging is how the spacecraft interacts with the plasma environment that causes charging.[2)] A spacecraft accumulates charge and adopts potential in response to interaction with the plasma environment. The key parameters in modeling spacecraft charging are the electron emission properties of insulating, such as the secondary electron emission (SEE) coefficient, photo emission (PE), and the surface and bulk conductivity of metal, and insulating materials. These parameters determine how much charge will accumulate in key spacecraft components in response to incident electron, ion and photon fluxes. It has been recognized that atomic oxygen present in low-Earth orbit (LEO) is one of the most important hazards to the spacecraft polymeric material, resulting in modification of the surface properties of the materials.[2-4)] Thus the interaction of LEO AO with the outer surfaces of a satellite may result in material degradation, modifying the chemical, electrical, thermal, optical and/or mechanical properties. This influences how charge will accumulate and redistribute across the spacecraft AO-modified surface, as well as the time-scale for charge transport and dissipation. This paper focuses on the change in resistivity properties of polyimide, predominantly used for satellite surfaces due to exposure to LEO AO. Resistivity is a key material parameter input for analytic spacecraft charging models, such as the Multi-utility Spacecraft Charging Analysis Tool (MUSCAT), developed by Kyushu Institute of Technology (KIT) and Japan Aerospace Exploration Agency (JAXA). Especially, we focus on how to measure resistivity for space applications.

To measure the resistivity of a spacecraft insulator, the charge storage method developed by Frederickson et al. is the most suitable configuration for space-like environments.[5,6)] In this method, charge is deposited on the surface of an insulator and is allowed to migrate through the dielectric. With this configuration, one can measure volume resistivity. Further modification is introduced to measure surface and volume resistivity together by allowing the diffusion of charge on the dielectric surface, as well as its

* Currently at JAXA, Tsukuba, Japan

migration through the materials. In this study, we discuss a laser detonation source that produces LEO-type AO environment having less than 10eV similar to LEO. After the degradation of spacecraft surface materials due to exposure, surface properties such as bulk and surface resistivity are measured. A comparative study using exposed and virgin materials will give a more accurate prediction of charging and arcing processes that affect the spacecraft. We will use these data for the spacecraft charging and arcing simulation tool, MUSCAT, developed at our laboratory. This will enable more accurate and precise predictions of charging and arcing conditions for spacecraft through-out their lifetimes.

In this paper, we present a technique for measuring the surface and bulk resistivity of an AO-exposed sample, along with the necessary mathematical formulation used for calculating resistivity.

2. Experimental Setup and Calculations

2.1. AO generation and material exposure facility

The AO generation technique used in this study is based on the dissociation of molecular oxygen into AO, originally developed by Caledonia et al.[7,8] The molecular oxygen is introduced into a previously evacuated expansion nozzle by a fast-acting pulse valve, for which the time open is set to just fill the nozzle with oxygen gas. A pulsed CO_2 laser of 5.5 Joule is then used to break down the gas using a laser-supported detonation (LSD) wave to create high-temperature plasma near the throat region of the nozzle; hence generation of high-velocity AO in an evacuated hypersonic nozzle.[9] The plasma expands down the nozzle as a blast wave, ingesting and dissociating the gas in front of it, ultimately converting the thermal energy into directed velocity. The expansion is tailored so as to allow for electron-ion recombination without atomic recombination. Thus, each laser pulse produces a temporally narrow, high-flux pulse of oxygen atoms at the nozzle exhaust.[8]

This AO flux interacts with materials kept for exposure testing. The accelerated exposure test produces almost the same effect on the material surfaces as if exposed to the actual AO environment of a LEO. The exposed material is tested for charging properties such as bulk conductivity and surface conductivity. A schematic diagram of the AO chamber (Fig. 1) shows the different components for AO generation, exposure and detection.

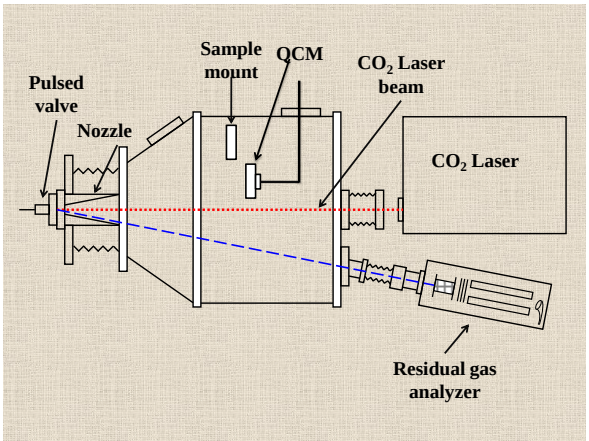

Fig. 1 Schematic diagram of the AO chamber

The chamber is comprised of two parts: the first part being conical and second part being cylindrical. An operating background pressure of 10^{-5} Pa, sufficiently low enough ensure collision-less passage of the energetic oxygen atom beam, is achieved using a turbomolecular pump (TMP) at 2230l/sec in conjunction with a rotary pump.[10,11] With this pumping system, the system operates up to 10Hz. A CO_2 pulsed laser provides 5.5J of energy per pulse at a wavelength of 10.6μm to dissociate the molecular oxygen. The laser pulse is focused on the nozzle tip using a ZnSe lens where the dissociation of molecular oxygen into AO happens. The molecular oxygen gas released from the cylinder using the pulse valve is injected into the nozzle in a controlled and measured amount using a mass flow controller.

2.2. AO diagnostic system

The complete AO exposure facility is shown in Fig. 2 with different components, such as CO_2 laser, residual gas analyzer (RGA), nozzle, pulse valve (PV), O_2 gas cylinder and AO generation chamber.

1. AO beam diagnosis is done using the RGA in single-mass mode, and a spectroscope analyse the AO generation beam.[10-12] AO generation is confirmed using the spectrometer to monitor the transition of neutral oxygen atoms at 777.3nm. This tracer radiation is produced through deexcitation.

2. The translational energy, and hence the velocity of AO species in the beam, are calculated using time of flight (TOF) distribution.[10,11] The RGA is a mass spectrometer of small physical dimension, is enclosed in a separate chamber and pumped separately using a TMP. TOF is calculated by dividing the distance between the pulse valve and RGA head by the duration between the laser triggering time and the arrival of the AO beam on the RGA head that appears on the RGA signal.

3. The flux, and hence the fluence of the generated AO, is measured using polyimide mass loss. A quartz crystal coated with polyimide is used for AO flux measurement. The flux per shot is about 4.2×10^{13} atoms/cm^2. The laser system was

set 2 Hz for 132,000 shots for the current test sample, hence the total fluence was 5.4 x 10^{18} atoms/cm^2.

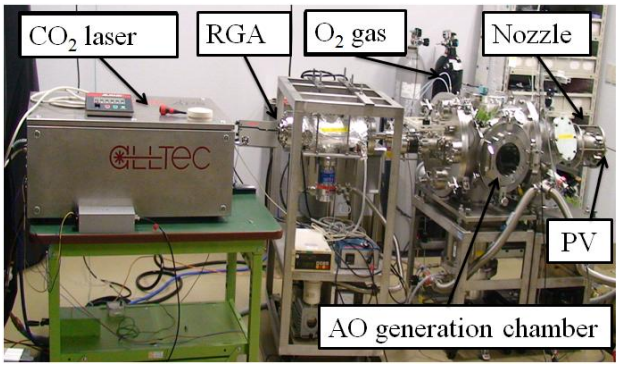

Fig. 2 Various components of the AO generation chamber.

Figure 3 depicts the TOF and the velocity distribution profile of AO at the RGA head, which is measured using the principle discussed above. The AO generated moves at the peak velocity of about 10-12km/s.

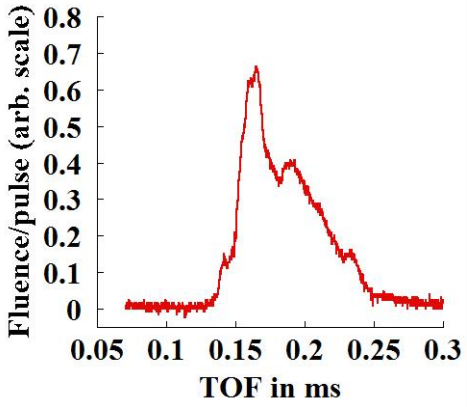

(a) Time of flight profile

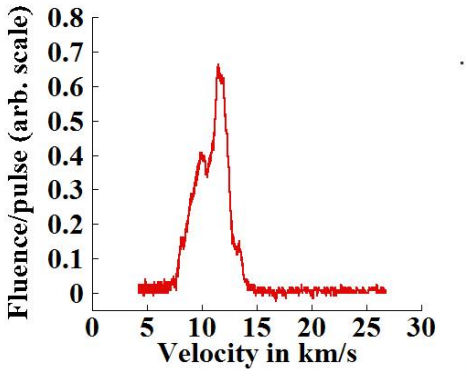

(b) Velocity profile

Fig. 3 TOF and velocity distribution of oxygen atoms at the RGA head for m/q= 16.

2.3. Resistivity measurment system

The resistivity of the sample is measured using the charge storage decay method. This method exposes one side of the insulator in a vacuum environment to a charge source, with a metal electrode attached to the back and front sides of the insulator for measuring surface and volume resistivity, respectively. These charges, deposited on the insulator surface, diffuse on the surface and migrate downward. Data are obtained by capacitive coupling to measure the resulting voltage (the electric field) due to the charge on the open surface. Measurements to determine resistance with this method require the use of an external charge deposition source and a very good electrostatic field probe.

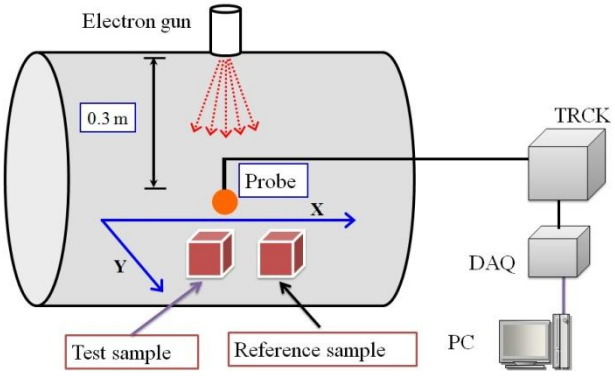

Fig. 4 Schematic view of resistivity measurement facility.

Figure 4 depicts the experimental setup and circuitry of the system. This chamber is also equipped with an electron gun (OME-0050LL), ensuring an electron shower with a maximum energy of 10keV, showing a maximum current density of not more than 100mAm^{-2}. The chamber is further equipped with a non-contacting surface potential meter (Trek, Model 341B), which is used to monitor the surface charge distribution of a sample with the help of a stage motor and movers. This allows the insulator surface to be scanned along a serpentine-like course within an area of 50x 50mm (step size 1mm).[13] A motor-driven shutter is located below the beam gun to expose the sample for the required time. The entire experiment is performed in a cylindrical shaped vacuum chamber of 0.6m diameter and 0.9m in length. This chamber is evacuated by a turbo-molecular pump (500l/s) which is backed by rotary pump to achieve a pressure in the range of 5.0x10^{-4}Pa.

2.4. Calculation of surface charge decay for resistivity measurement

In order to measure resistivity using the surface charge decay method, an insulator is assumed to be instantaneously charged at t=0 by an electron beam to produce certain surface potential, and this surface potential is monitored afterward using a surface potential meter. The insulator, having thickness τ, is attached with an electrode in such a way that it allows charge diffusion on the surface and through the material. Figure 5 shows that the test sample material is exposed to the electron beam at the center in radius r_0, and that the electron is allowed to diffuse in material of radius R. At the end of test material radius R, there is a metallic electrode connected to a highly conductive adhesive material to provide a path for electron flow from the test material to the electrode. The rate of change in the

surface charge density when irradiated by an electron beam of current density j is given by the following expression:

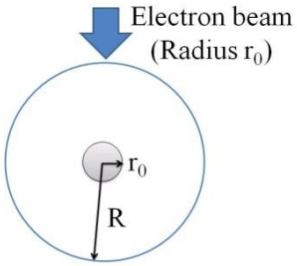

Fig. 5 Sketch showing method for calculating resistivity.

$$\frac{\partial \sigma}{\partial t} = -j(1-\delta) + \frac{1}{R_s}\nabla^2\phi - \frac{1}{\rho\tau}\phi \qquad (1)$$

Here, δ is the secondary electron coefficient, R_s is the surface resistance (Ω/□"sq") and ρ is the volume resistivity (Ωm). If σ is the electric charge density (Coulomb.meter^{-2}), ε is the permittivity (Coulomb.Volt^{-1}.meter^{-1}), ϕ is the surface potential and τ is the thickness, then the relation among these is as follows.

$$\sigma = \frac{\varepsilon\phi}{\tau} \qquad (2)$$

Therefore, it becomes a partial differential equation concerning the electrical potential distribution ϕ.

$$\frac{\partial \phi}{\partial t} = -\frac{j\tau}{\varepsilon}(1-\delta) + \frac{\tau}{\varepsilon R_s}\nabla^2\phi - \frac{1}{\rho\varepsilon}\phi \qquad (3)$$

The center of the beam is solved with the cylindrical coordinates system. Thus,

$$\nabla^2\phi = \frac{1}{r}\frac{\partial}{\partial r}\left(r\frac{\partial \phi}{\partial r}\right) \qquad (4)$$

Hence,

$$\frac{\partial \phi}{\partial t} = -\frac{j\tau}{\varepsilon}(1-\delta) + \frac{\tau}{\varepsilon R_s}\frac{1}{r}\frac{\partial}{\partial r}\left(r\frac{\partial \phi}{\partial r}\right) - \frac{1}{\rho\varepsilon}\phi \qquad (5)$$

This equation is used for fitting the potential decay curve to find the resistivity values. In Eq. [5], radius r_o does not appear explicitly, and the out radius of R appears as the boundary condition. Therefore, beam radius r_o, although defined in Fig. 5, has little meaning in the following analysis.

2.5. Resistivity measurement sample layout

Resistivity measurement is performed with the electrode configuration shown in Fig. 6. The electrode is made of a copper tape with a conductive adhesive. The adhesive provides a very good electrical contact between the polyimide and electrode. The test sample size is 60x 60mm and has a thickness of 25μm. After irradiating the electron beam on an area of Φ = 10mm at the center of the test sample as shown in Fig. 7, the charges are allowed to dissipate in Φ = 50mm. Potential drop on the sample surface is scanned using a surface potential meter. The surface potential meter scans the surface along a serpentine-like course with a distance resolution of 1mm. The sample distance from the surface potential meter is about 2mm.

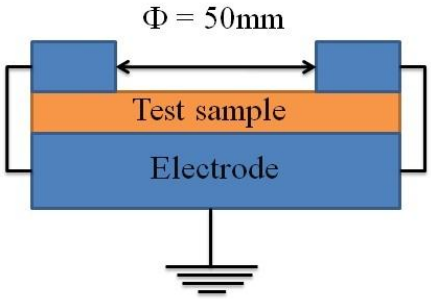

Fig. 6 Electrode configuration for measuring surface and volume resistivity.

Figure 7 shows the experimental setup for resistivity measurement of a sample inside the chamber. The electron beam enters vertically downward and is allowed to irradiate at the sample center using two beam modifier plates. Hole sizes of 5mm and 10mm in beam modifier plates are used to expose respective areas of 5mm and 10mm in diameter at the center of the test sample directly to the electron beam. Once the electron beam irradiates the sample center for 1min, electron beam exposure is stopped. Afterward, the surface potential meter scans the test sample surface at a regular interval using the moveable stage.

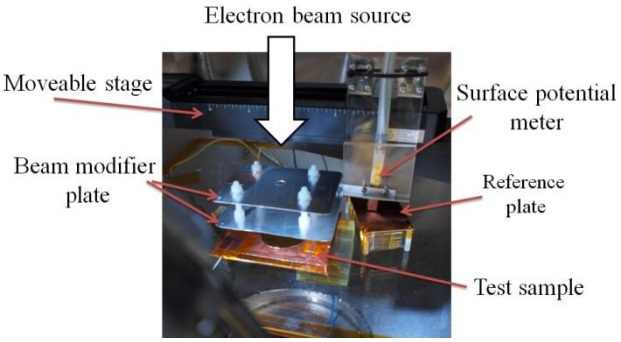

Fig. 7 The experimental setup for resistivity measurement of the sample inside the chamber.

3. Results and Discussion

3.1. Effect of AO exposure on materials

AO exposure changes the surface structure of materials. It may influence the surface properties that play an important role in spacecraft charging. In this paper, we studied the change in surface morphology of polyimide using a scanning electron microsocope (SEM). The SEM images prior to AO exposure and after exposure are shown in Fig. 8. The sample surface is smooth prior to AO exposure (virgin polyimide). The surface morphology of AO exposed to

polyimide was found to change when it is exposed to a fluence of 5.4x 10^{18}atoms/cm^2. This fluence value is equivalent to 10 years of AO exposure at an altitude of 800km and velocity of 10-12km/s. The fluence value can be normalized for the condition of 8km/s in a LEO, in accordance with Tagawa et al. findings.[14] In Fig. 8(b), the size of a typical granular structure is 30nm. It is obvious that the surface morphology of the polyimide sample becomes much rougher and is significantly modified. This shows that AO surface erosion is significant for the given AO fluence.

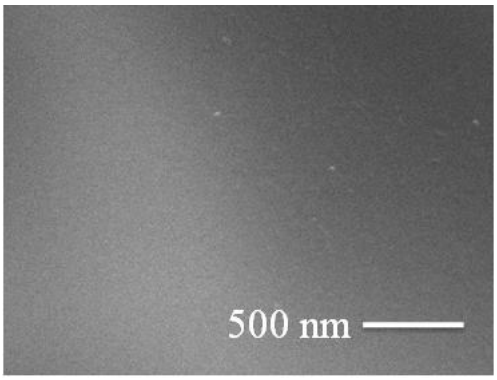

(a) Virgin polyimide

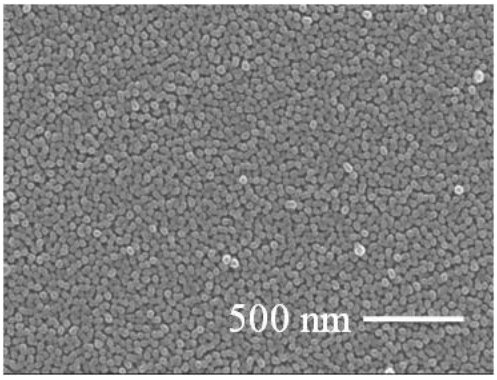

(b) AO exposed polyimide

Fig. 8 SEM of virgin and AO-exposed polyimide.

3.2. Surface potential distribution

Surface potential distribution was measured regularly for 96hr. The change in surface potential distribution was monitored and displayed in a two-dimensional graph assuming a rotation-symmetric shape. Figure 9(a) and 9(b) show the potential distribution view for virgin and AO-exposed samples, respectively, along the Y axis as recoded by a surface potentiometer for 0 (just after electron beam stop), 24 and 96hr after electron beam exposure. It shows that the potential is almost symmetrically distributed on the surface along the center of electron beam exposure. After the electron beam is stopped, the potential decays as the charge diffuse outward the ring electrode and migrates downward to the bottom electrode. To determine the surface and volume resistivity, these potential distribution patterns are used. The 24hr case is used as the initial condition for simulation using Eq. (5), and 96hr case is used for comparison between experimental and simulation results.

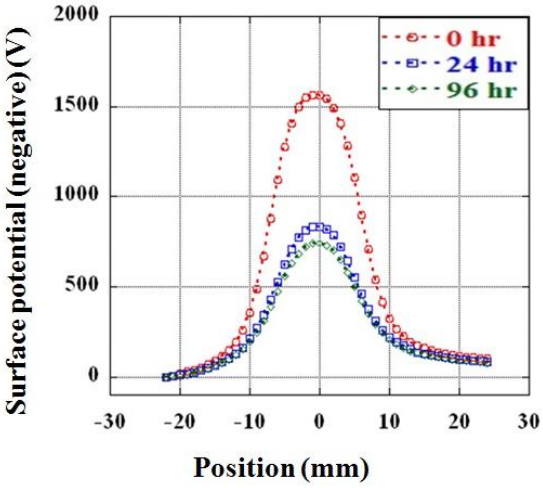

(a) Surface potential decay of virgin sample

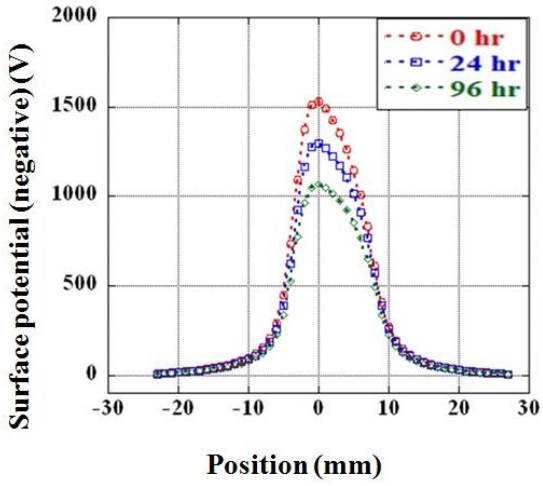

(b) Surface potential decay of AO exposed sample

Fig. 9 Measured surface potential decay on virgin and AO-exposed polyimide when measuring resistivity with the sample layout shown in Fig. 6.

Figure10 and 11 show a three-dimensional view of the surface potential decay profile for the virgin and AO-exposed polyimide, respectively. They show that the surface potential decay profile is axis-symmetric in pattern. The potential patterns are shown for four cases of time delay, 0hr (just after electron beam irradiation), 10hr, 24hr and 96hr electron beam irradiation was stopped.

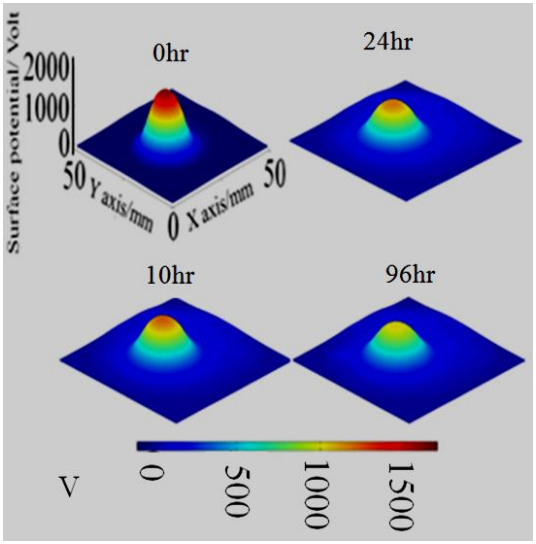

Fig. 10 Surface potential decay profile of virgin polyimide measured using a surface potentiometer.

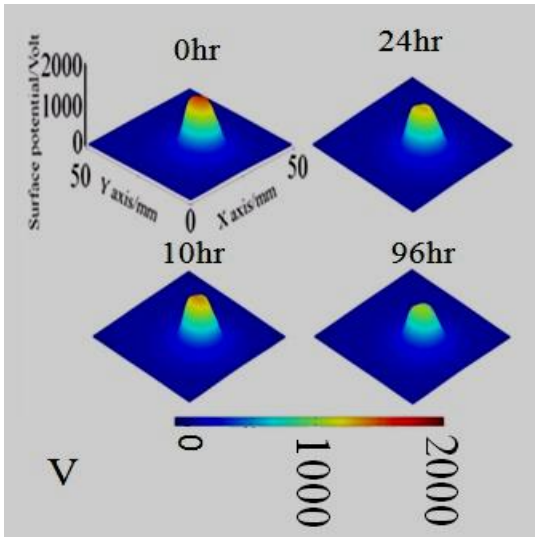

Fig. 11 Surface potential decay profile of AO exposed polyimide measured using a surface potentiometer.

3.3. Determination of surface and volume resistivity

A resistivity measurement experiment was performed for virgin and AO-exposed polyimide samples. Three experiments were performed for the same virgin samples with hole sizes in the beam modifier plate of 5mm, 10mm and 10mm in diameter, respectively, for exposing the electron beam directly to the corresponding area at the center of the sample. One of the experiments was performed for an AO-exposed sample with a hole size of 10mm in the beam modifier plate. After electron beam exposure, the surface potential of the test sample was recorded regularly using a surface potentiometer. Figure 12 shows the surface potential drop at the center of the test sample surface as time progressed. This shows that there are two significant features of potential drop profiles.

The initial surface potential drop is due to polarization-depolarization phenomena. After a certain time, the process of depolarization ends. After the initial depolarization phenomenon finishes, there is a further drop in surface potential due to electrons propagating outward towards the peripheral electrode and through the bulk of materials. After a certain time, the flow of electrons from the sample center to the peripheral electrode and through the bulk materials becomes steady. We consider the beginning of this time as 24hr after the electron beam irradiation stopped, as shown in Fig. 12. This area of conductivity is called "dark current conductivity", and is assumed to be constant and independent of time.[5)]

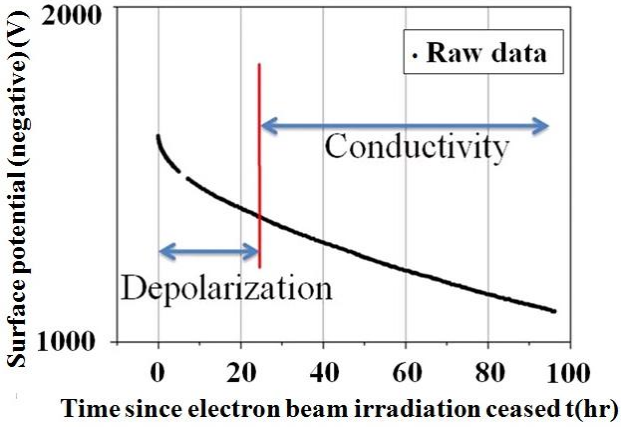

Fig. 12 Temporal profile of the potential at the center of the test samples.

At the point of 24hr after electron beam stoped, the potential decay profile was fitted using Eq. (5). We used the potential profile, along the Y axis passing through the center, at 24hr as the initial condition and solved Eq. (5) numerically unto 96hr. The numerical profile at 96hours was compared with the experimental data. We varied the surface and volume resistivity in Eq. (5) and looked for a combination of the two values to give the best fit between the simulation and experiment. For the purpose of analysis, each potential profile, as shown in Fig. 9, was divided into two sections, one in negative X-axis and other in positive X-axis with the peak potential point as the origin of X-axis. The numerical technique used to solve Eq. (5) is a finite difference method, where the forward difference and the central difference are used for the temporal and spatial difference, respectively. The temporal step was 10seconds and the spatial step was 1mm.

In terms of space application, evaluating the resistivity at the later stage of potential decay gives a safe margin to the prediction of charging in orbit. Until Frederickson et al. gave warning[6)], the majority of spacecraft charging analysis was carried out using the resistivity values measured based on conventional methods, such as the American Society for Testing and Materials (ASTM) D-257 standard, where the resistivity value measured after 1min of voltage application is used as the resistivity. The time of 1minute is when polarization dominates the resistivity is underestimated. As shown in the experimental results in Fig. 12, the charge does

not decay as quickly as the initial decay phase where polarization dominates.

In spacecraft charging, charging of the insulator continues for a time scale of seconds to hours. The measurement results shown in this paper tell us that the charge can stay even for days after the end of the charging event. The remaining charge is then added as the initial charge in the next charging event. To make a conservative prediction of spacecraft charging, it is safer to use the value evaluated in this research.

The analysis results for the simulation of Eq. (5) and experimental results of potential decay for AO-exposed sample are shown in Fig. 13. In this figure "Initial" means the surface potential 24hr after the electron beam was stopped, (i.e., the curves marked as "24hr" in Fig. 9), which was chosen as the starting time for the simulation. In this figure, "Exp" shows the surface potential after 96hr and "Simulation" shows the surface potential calculated using Eq. (5). We assumed a certain set of the volume and surface resistivity and solved Eq. (5) and looked for a combination that matches best with the experimental results. The search of the best combination was carried out in a two-dimensional space made of the surface and volume resistivity, whose ranges were 10^{12} and 10^{20} in logarithmic scales for both values. The two-dimensional space was divided into 160x160 points, and simulations were carried out for each point. This shows that the simulation plot and experimental plot match each other for 96hr, verifying Eq. (5).

In Table 1 and Table 2, we list the surface and volume resistivity of the virgin and AO-exposed samples. Each potential distribution pattern is divided into two sections for simulation analysis. They consist of the right and left sides of the curve across zero in Fig. 9. Therefore, for each experiment, two sets of resistivity values were derived.

Table 1. Surface resistivity of the virgin and AO-exposed samples

Sample condition	Experiment No.	Surface resistivity 10^{17} Ω/□	Avg. 10^{17} Ω/□	Standard deviation 10^{17} Ω/□
Virgin	1 (5mm)	2.8	2.3	0.92
		3.6		
	2 (10mm)	2.8		
		1.8		
	3 (10mm)	1.3		
		1.4		
AO-exposed	4 (10mm)	4.5	5.8	1.8
		7.1		

Table 2. Volume resistivity of the virgin and AO-exposed samples

Sample condition	Experiment No.	Volume resistivity 10^{16} Ωm	Avg. 10^{16} Ωm	Standard deviation 10^{16} Ωm
Virgin	1 (5mm)	1.0	2.2	1.1
		0.89		
	2 (10mm)	2.2		
		2.2		
	3 (10mm)	3.1		
		3.5		
AO-exposed	4 (10mm)	1.8	1.7	0.14
		1.6		

The standard deviations were calculated using the six values for the virgin polyimide and two values for the AO-exposed polyimide.

The value of surface resistivity was found to increase whereas volume resistivity was found to be the same for virgin and AO-exposed samples. This shows that AO exposure affects the value of surface resistivity by a factor of more than two, but does not affect volume resistivity for the given fluence. The increase in surface resistivity can be due to the roughening of the surface by the AO beam, as observed in the SEM images (Fig. 8). This roughening of the sample due to AO-exposure will increases the net distance that the electrons have to travel on the material surface, hence producing higher resistivity to the electron flow. The difference in the value of volume resistivity is not significant as the average value of the AO-exposed sample is within one standard deviation from the average of the virgin sample.

No change in volume resistivity is reasonable considering that AO-exposure affects the surface morphology, not the bulk properties or bulk structure of the material.

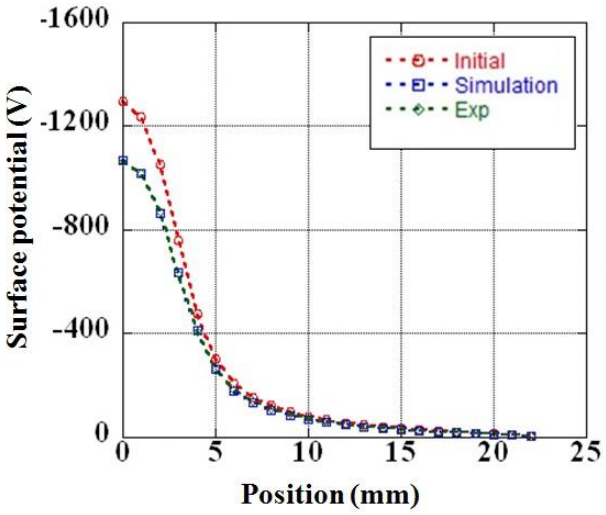

Fig. 13 Comparison of potential decay between experiment and simulation.

4. Conclusion

Surface charge decay method, for simultaneous investigation of surface and volume resistivity, with the given electrode configuration was found suitable for dielectric materials. Result applying the mathematical formula discussed also show good agreement with the experimental data. It was observed that AO-exposure affects surface resistivity, but does not affect volume resistivity for the given AO fluence. Since surface resistivity is dependent on the surface structure, it is affected by AO exposure. The value of volume resistivity is quite high, so changes in surface morphology due to AO fluence do not have significant effect on volume resistivity as this depends on the bulk materials. Spacecraft charging simulation tools like MUSCAT should use the same volume resistivity value and change the surface resistivity value to simulate charging environment at the end of satellite life as it is used at the beginning of life simulation.

In the near future, we will increase the number of samples by changing the AO exposure fluence to quantify the change in surface resistivity. Other spacecraft insulator materials will also be tested to determine the differences among materials. A detailed analysis of the surface will be also necessary to investigate the mechanism of change in resistivity.

Acknowledgements

The authors are very thankful to the Japanese Ministry of Education, Sport, Culture, Science and Technology for providing funds for this research, and to Prof. M. Tagawa, Kobe university, Japan, for providing valuable guidance at different stages.

References

1) Hatta, S., Muranaka, T., Kim, J., Hosoda, S., Ikeda, K., Kurhara, N., Cho, M., Ueda, H., Koga, K. and Goka, T.: Accomplishment of Multi-utility Spacecraft Charging Analysis Tool (MUSCAT) and its Future Evolution, *Acta Astronautica*, **64**, 5-6 (March-April 2009), pp 495-500.
2) Reddy, M. R.: Review Effect of Low Earth Orbit Atomic Oxygen on Spacecraft Materials, *Journal of Materials Science*, **30**(1995), pp. 281-307.
3) Zhao, X. H., Shen, Z. G., Xing, Y. S. and Ma, S. L.: An Experimental Study of Low Earth Orbit Atomic Oxygen and Ultraviolet Radiation Effect on Spacecraft Materials-Polytetrafluoroethylene, *Polymer Degradation and Stability*, **88**(2005), pp. 275-285.
4) Yokota, K. and Tagawa, M.: Comparison of Polyethlene and Polymide as a Fluence Monitor of Atomic Oxygen, *Journal of Spacecraft and Rockets*, **44**, 2(2007), pp. 434-438.
5) Dennison, J. R., Bruson, J., Swaminathan, P., Wesley, N. and Frederickson, A. R.: Method of High Resistivity Measurement Related to Spacecraft Charging; *IEEE Transaction on Plasma Society*, **34** (2006), pp. 2204-2218.
6) Frederickson, A. R. and Dennison, J. R.: Measurement of Conductivity and Charge Storage in Insulators Related to Spacecraft Charging, *IEEE Transactions on Nuclear Science*, **50**,6 (2003), pp. 2284-2291.
7) Caledonia, G. E. and Krech, R. H.: Studies of the Interaction of 8km/s Oxygen Atoms with Selected Materials, 20th Intersociety Conference on Environmental Systems, SAE Technical Paper Series, 901411, 1990.
8) Caledonia, G. E., Krech, R. H. and Green, B. D.: A high Flux Source of Energetic Oxygen Atoms for Material Degradation Studies, *AIAAJjournal*, **25**, 1(1987), pp. 59-63.
9) Caledonia, G. E., Krech, R. H., Green, B. D. and Pirri, A. N.: Source of High Flux Energetic Atoms, United States Patent, Patent Number: 4,894,511, Jan 16, 1990.
10) Mundari, N. D. A., Okumura, T., Iwata, M., Toyoda, K. and Cho, M.: Atomic Oxygen Facility Simulating LEO AO Environment for Material Exposure to Understand Charging-Arcing Behavior of Exposed Surface Materials, 60th International Astronautical Congress, Daejeon, , IAC-09C.6.9, 2009.
11) Mundari, N. D. A., Chiga, M., Okumura, T., Khan, A. R., Masui, H., Iwata, M., Toyoda, K. and Cho, M.: Generation of LEO-type Atomic Oxygen Environment in Laboratory for Charging Property Database, 27th ISTS, , 2009-c-03, 2009.
12) Cazaubon, B., Paillous, A., Siffre, J. and Thomas, R.: Five Electron-Volt Atomic Oxygen Pulsed Beam Characterization by Quadrupolar Mass Spectrometer, *Journal of Spacecraft and Rockets*, **33**, 6 (1996), pp. 870-876.
13) Lutz, B. and Kinddersberger, J.: Determination of Volume Resistivity of Polymeric Insulators by Surface Charge Decay, proceeding of 16th International symposium on High Voltage Engineering. ISBN 978-0-620-44584-9 , 2009.
14) Tagawa, M., Yokota, K., Kishida, K., Okamoto, A. and Minton, T. K.: Energy Dependence of Hyperthermal Oxygen Atom Erosion of a Fluorocarbon Polymer: Relevance to Space Environmental Effects, *ACE Appl. Mater. Interface*, **2**, 7 (2010), pp. 1866-1871.